https://ntrs.nasa.gov/search.jsp?R=19660027981 2020-03-16T17:37:34+00:00Z

A THEORETICAL STUDY OF THE GAMMA-RAY SCATTERING TECHNIQUE FOR MEASURING ATMOSPHERIC DENSITY

GPO PRICE $ _____

CFSTI PRICE(S) $ _____

Hard copy (HC) 2.50

Microfiche (MF) .75

ff 653 July 65

Final Report
August 1966

R. P. Gardner and D. R. Whitaker

(Distribution of this report is provided in the interest of information exchange. Responsibility for the contents resides in the author or organization that prepared it.)

Prepared for

Langley Research Center
National Aeronautics and Space Administration

(Prepared under Contract No. NAS1-5467, RTI Project No. NU-239, by the Measurement and Controls Laboratory of the Research Triangle Institute, Durham, North Carolina)

FACILITY FORM 602

N66 37271 (ACCESSION NUMBER)

58 (PAGES)

CR-66142 (NASA CR OR TMX OR AD NUMBER)

(THRU) 1

(CODE) 24

(CATEGORY)

N66-37271

Errata for NASA Contractor Report No. 66142

A THEORETICAL STUDY OF THE GAMMA-RAY SCATTERING TECHNIQUE FOR MEASURING ATMOSPHERIC DENSITY

R. P. Gardner and D. R. Whitaker

August 1966

1. "NASA Model IV" should be replaced by "Mars Model Atmosphere VM-4" on page 20, line 15; page 20, line 18; page 21, line 3; page 21, line 11; page 22, line 23, and on Figure 4 on page 39.
2. "of atomic weight" should be replaced by "to atomic weight" on page 20, line 23.
3. Reference 4 on page 34 should be: Anon., "Comparative Studies of Conceptual Design and Qualification Procedures for a Mars Probe/Lander," Vol. V, Book 1, p. 78, AVSSD-0006-66-RR, Avco. Corp. (1966).
4. The cover page should have "NASA Contractor Report No. 66142" inserted in the upper right-hand corner.

TABLE OF CONTENTS

1. SUMMARY

This report describes a theoretical, mathematical modeling study of the gamma-ray scattering technique for measuring atmospheric density. A basic model was derived which describes the response of this technique in a cylindrically symmetrical geometry like that used to date in prototype gauges flown in Nike-Apache vehicles. Two other models were derived to describe the response of a gauge of this type in a steel wall vacuum sphere and the response to gamma-ray streaming down the rocket walls. An existing Monte Carlo calculation was used to calculate shield effectiveness.

The predicted gauge response was linear with atmospheric density, independent of atmospheric composition if gamma-ray energies larger than 0.1 Mev are employed, effected by atmospheric density as far as 10 meters from the rocket, and independent of shock wave density perturbations that are likely to be encountered. The sensitivity of the gauge is at a maximum for air at a gamma-ray energy of .038 Mev and depends on the reciprocal of the source-to-detector distance.

The significant problems identified are: (1) inaccurate calibration technique, (2) a high background response due to gamma-ray streaming down the rocket wall, and (3) a dependence on atmospheric composition if gamma-ray energies less than 0.1 Mev are used. The shield effectiveness was found to be adequate.

A calibration technique involving the use of the present models with calibration data taken in two spheres of different sizes is suggested.

2. INTRODUCTION

The gamma-ray scattering technique shows promise of being able to determine the atmospheric density surrounding a space vehicle. In this connection it has several major advantages over most other possible techniques. These include: (1) fast response time, (2) the source and detection equipment necessary can be installed entirely within the space vehicle, (3) large effective sample volume, (4) linear response in the density region of interest, and (5) the response can be made to be essentially independent of the atmospheric composition.

Some feasibility work to the prototype phase has been funded to demonstrate the use of this technique to measure the atmospheric density of the Earth at various altitudes. Several problem areas have become apparent in the tests of these prototypes. Some of these problems are: (1) an unpredicted high background response of unknown origin, (2) the lack of an accurate calibration method, and (3) the general lack of a theoretical treatment of the technique which would allow the optimum design of an instrument.

In the present program we have undertaken a theoretical, mathematical modeling treatment of the gamma-ray scattering technique for measuring the atmospheric density surrounding cone-shaped rockets. In particular we have considered the case in which a source, a conical shield, and a cylindrical scintillation detector are mounted on the major axis inside a cone-shaped rocket. Our purpose is to study the problem areas listed in the previous paragraph. The specific problem areas identified by the Work Statement are: (1) atmospheric composition variation, (2) atmospheric density variation, (3) container composition and thickness effects, (4) source energy and placement effects, and (5) calibration corrections and shielding effectiveness to include analysis of typical X-ray backscatter payload data. On the basis of our results we are to indicate the areas in which problems may arise if the gamma-ray scattering technique is to be used on a Mars Probe and shall suggest potential means of solving these problems.

3. SYMBOLS

A	atomic weight of an element
a	a constant
a_1	slope of the rocket wall
a_2	intercept of rocket wall
b	a constant
d	source-to-detector distance
d_i	detector diameter
d_l	detector length
D	fractional number of gamma rays of a certain energy and direction
E	gamma-ray energy
$\bar{E}$	effective gamma-ray energy
h	Planck's constant
i	subscript that refers to a particular element
K	a constant
n	total number of elements in the atmosphere
P_1, P_2, P_3, P_4	probabilities that are pertinent to particular parts of a gamma-ray path
R	gauge response
R_s	gauge response inside a calibration sphere
R_a	gauge response to atmospheric scattering
R_{bs}	gauge response to gamma rays that penetrate the shield
R_{bss}	gauge response to gamma rays that stream down the rocket wall
r	distance from source to a scattering point in the atmosphere
r_a	distance through atmosphere
r_{max}	maximum distance of model integration
r_o	classical radius of electron
r_s	distance through shock wave

r_w distance through wall

T_{max} maximum energy imparted to an electron by a Compton scattering interaction with a gamma ray

t_w rocket wall thickness

w weight fraction of an element

$\bar{x}$ horizontal distance from source to effective interaction point

$\bar{y}$ vertical distance from source to effective interaction point

Z atomic number of an element

Greek Letters

α ratio of gamma-ray energy divided by the rest-mass energy of an electron

μ total attenuation coefficient

ν wave length of gamma ray

ϕ angle between path of gamma ray and central axis of rocket

ρ density

σ Compton scattering coefficient

τ photoelectric effect coefficient

θ angle of gamma-ray scatter

4. DERIVATION OF MATHEMATICAL MODELS

In the course of this study a mathematical model was used for general study of the gamma-ray scattering principle for measuring atmospheric density. This model was modified for studying the specific problems of calibration in spheres and the streaming of gamma rays down the rocket wall. In addition an existing Monte Carlo treatment was used to determine the shield effectiveness. The derivations of the first three models and a summary description of the last are included in this section.

4.1 Model of Gamma-Ray Scattering Principle for Measuring Atmospheric Density

A mathematical model of the gamma-ray scattering principle for measuring atmospheric density has been derived which treats the case of single gamma-ray scattering in a geometry which is symmetrical about the axis of the gamma-ray source and detector (cylindrically symmetrical). Refer to Fig. 1 for a schematic drawing and the coordinates of the system treated. This model essentially consists of mutually-exclusive probabilities that describe separate parts of the path of any gamma ray that is emitted from the source, scattered by the surrounding atmosphere toward the detector, and is detected. The product of these separate probabilities integrated over the total volume of interaction represents the response of the gamma-ray gauge. Spherical coordinates with origin at the source are used throughout.

The first probability P_1 is that a gamma ray is emitted within a differential angle $d\phi$ at a mean angle ϕ from the source-detector axis and reaches the distance r without being attenuated.

$$P_1 = (\tfrac{1}{2}) \sin \phi \exp(-\mu r)\, d\phi \qquad (4.1\text{-}1)$$

where ϕ is the angle between the direction of the gamma-ray and the axis of the source and detector, in radians,

μ is the attenuation coefficient, in cm^{-1},

and r is the distance from the source, in cm.

The attenuation coefficient for a given material is the sum of the total Compton scattering probability and the photoelectric effect probability. The probability for pair production is not considered since this probability is negligible for gamma-ray energies less than about 2 Mev.

$$\mu = \sigma + \tau \qquad \text{cm}^{-1} \tag{4.1-2}$$

where σ is the total Compton scattering probability, in cm^{-1},

and τ is the photoelectric effect probability, in cm^{-1}.

The total Compton scattering probability is given by:

$$\sigma = \sigma_e N \rho \sum_{i=1}^{i=n} w_i Z_i / A_i \qquad \text{cm}^{-1} \tag{4.1-3}$$

where σ_e is the total Compton scattering probability per electron, in $\text{cm}^2/\text{electron}$,

N is Avogadro's Number, 6.025×10^{23} atoms/g-atom,

ρ is the density, in g/cm^3,

w_i is the weight fraction of element i,

Z_i is the atomic number of element i,

A_i is the atomic weight of element i,

and n is the total number of elements.

The total Compton scattering probability per electron is given by Evans[1] as:

$$\sigma_e = 2\pi r_o^2 \left\{ \frac{1+\alpha}{\alpha^2} \left[\frac{2(1+\alpha)}{1+2\alpha} - \frac{1}{\alpha} \ln(1+2\alpha) \right] + \frac{1}{2\alpha} \ln(1+2\alpha) - \frac{1+3\alpha}{(1+2\alpha)^2} \right\} \text{cm}^2/\text{electron} \tag{4.1-4}$$

where r_o is the classical electron radius, 2.818×10^{-13} cm,

and α is the gamma-ray energy in Mev divided by the rest-mass energy of

an electron (.511 Mev).

The photoelectric effect probability is given by:

$$\tau = N\rho \sum_{i=1}^{i=n} w_i \tau_{ai} / A_i \qquad cm^{-1} \tag{4.1-5}$$

where τ_{ai} is the photoelectric effect probability per atom of element i for a gamma ray of a given energy, in cm^2/atom.

The photoelectric effect probability per atom can be approximated (c.f. Evans[1]) for any element at any gamma-ray energy by the empirical relation:

$$\tau_{ai} = \frac{K Z_i^a}{E^b} \qquad cm^2/atom \tag{4.1-6}$$

where K, a, and b are empirical constants,

and E is the gamma-ray energy, in Mev.

The constant a is in the range from 4.2 to 4.6 while b is about 3.5. Equation (4.1-6) is substituted into Eq. (4.1-5) to give:

$$\tau = \frac{KN\rho}{E^b} \sum_{i=1}^{i=n} w_i Z_i^a / A_i \qquad cm^{-1} \tag{4.1-7}$$

The attenuation of the gamma-ray beam to the point r consists of the attenuation through the wall, the attenuation through a shock wave, and the attenuation through the atmosphere. If the fractional part of the distance r and the density and the composition are known for each of these three media, then the exponential term in Eq. (4.1-1) can be calculated from:

$$\exp(-\mu r) = \exp(-\mu_w r_w - \mu_s r_s - \mu_a r_a) \tag{4.1-8}$$

where w refers to the rocket wall,

s refers to the shock wave,

and a refers to the atmosphere proper.

The second probability P_2 is that the gamma ray reaching the point at r and ϕ is scattered from within the differential distance dr between angles θ_1 and θ_2 to intersect the detector.

$$P_2 = N\rho \left[\sum_{i=1}^{i=n} w_i Z_i / A_i \right] [\sigma_e(\theta_1) - \sigma_e(\theta_2)] \left(\frac{d_x}{2\pi S_x} \right) dr \qquad (4.1\text{-}9)$$

where $\sigma_e(\theta_1)$ is the integral of the differential Compton scattering probability per electron from $\theta = 0$ to $\theta = \theta_1$, in cm^2/electron,

S_x is the radius of the circle formed by rotation of s extended so that it intersects the detector about the line r at the angle $(\theta_1 + \theta_2)/2$, in cm,

and d_x is the length of the circle circumference formed by rotation of S_x that is intercepted by the detector, in cm.

The term $[\sigma_e(\theta_1) - \sigma_e(\theta_2)]$ is approximated well (c.f. Evans[1]) when $\theta_1 - \theta_2$ is small by:

$$[\sigma_e(\theta_1) - \sigma_e(\theta_2)] = \pi r_o^2 \sin\theta_a (h\nu'/h\nu_o)^2 [h\nu'/h\nu_o + h\nu_o/h\nu' - \sin^2\theta_a](\theta_1 - \theta_2) cm^2/\text{electron} \qquad (4.1\text{-}10)$$

where θ_a is the average angle $(\theta_1 + \theta_2)/2$,

$h\nu_o$ is the original energy of the gamma ray, in Mev,

and $h\nu'$ is the energy of the gamma ray after it is scattered through the angle $(\theta_1 + \theta_2)/2$, in Mev.

The terms d_x and S_x must be found by first obtaining the point on the detector at which the line s forms a tangent with the detector surface as it is rotated about r.

The third probability P_3 is that the gamma-ray beam described by P_2 is not attenuated before it reaches the detector. Since the gamma rays in this beam have been scattered, the attenuation coefficient must be that for the scattered energy.

$$P_3 = \exp(-\mu' s) \qquad (4.1\text{-}11)$$

where μ' is the attenuation coefficient for the gamma ray scattered at angle $(\theta_1 + \theta_2)/2$, in cm^{-1},

and s is the distance from the point at r and ϕ to the top center of the detector, in cm.

The energy of the scattered gamma ray (c.f. Evans[1]) is obtained from the relation:

$$h\nu' = \frac{h\nu_o}{1 + (1 - \cos\theta)(h\nu_o/0.511)} \qquad (4.1\text{-}12)$$

The attenuation coefficient μ' is then obtained as was μ from Eqs. (4.1-2) through (4.1-8).

The fourth and final probability P_4 is the detector efficiency or the probability that the gamma ray which intercepts the detector will give rise to a measured pulse. This probability is a function of the detector size and material, the gamma-ray energy, and the discriminator settings on the electronics used to process the pulses from the detector. For a given detector with fixed discriminator settings, P_4 is given by:

$$P_4 = f(E) \qquad (4.1\text{-}13)$$

where $f(E)$ is a function of the gamma-ray energy.

Since the primary interest in this program is in the use of scintillating crystals for detection, a generalized form of $f(E)$ was derived for this case. Scintillating crystals convert to a pulse of light a proportional amount of that energy from a gamma-ray interaction that is imparted to the participating electron. Both the photoelectric effect interaction which imparts all of the gamma-ray energy to an electron and the Compton scattering interaction (or multiple Compton scattering interactions) which can impart any energy up to a maximum dictated by the original

energy of the gamma ray can occur in any single interaction of a gamma ray with a scintillating crystal. A typical spectrum of the light pulses that have been converted to voltage pulses (pulse-height spectrum) from a monoenergetic source of gamma rays interacting with a scintillating crystal is shown in Fig. 2. The photopeak and Compton continuum are identified. The area under this curve divided by the number of gamma rays that intercepted the detector is the total efficiency E_t of the crystal for the particular gamma-ray energy illustrated. The fraction of the total area in the photopeak is called the photofraction, denoted F_p. These parameters as a fraction of gamma-ray energy were taken from the book by Crouthamel[2].

For the present purpose the shape of the photopeak is taken as a normal (or Gaussian) distribution with a standard deviation that can be chosen to fit the crystal being used, while that under the Compton continuum is taken as a rectangular distribution with an upper limit of the maximum energy that can be imparted to an electron by a gamma ray of the energy employed in one Compton scattering interaction. This maximum electron energy T_{max} (c.f. Evans[1]) is given by:

$$T_{max} = \frac{2(h\nu)^2}{0.511 + 2h\nu} \qquad (4.1\text{-}14)$$

Data is available in the literature[2] for total efficiencies and photofractions as a function of crystal size, crystal material, and gamma-ray energy. With this data one can calculate the efficiency for a given crystal operated between any two energy-discrimination levels for any gamma-ray energy by using the assumptions made about the shape of the pulse-height spectrum in the previous paragraph.

The response of the gamma-ray gauge per source disintegration is given by:

$$R = \int_r \int_\phi P_1 P_2 P_3 P_4 \qquad (4.1\text{-}15)$$

Equation (4.1-15) was evaluated from $r = o$ to $r = r_{max}$ and from $\phi = \phi_{min}$ to $\phi = \phi_{max}$

by a computer-programmed, finite-difference integration. About 1000 increments of equal size were taken to insure an accurate solution. The finite-difference form of Eq. (4.1-15) is:

$$R = \Delta r \, \Delta \phi \sum_i \sum_j (P_1/d\phi)_{ij} (P_2/dr)_{ij} (P_3)_{ij} (P_4)_{ij} \qquad (4.1\text{-}16)$$

where i refers to a mean value of ϕ in each $\Delta \phi$ increment,

and j refers to a mean value of r in each Δr increment.

In addition to the gauge response, the first moments about the source of the contribution from each volume increment were taken as functions of the x and y distances from the origin and the energy of the detected gamma ray. These relations in finite-difference form are:

$$\bar{x} = \frac{\Delta r \Delta \phi}{R} \sum_i \sum_j x_{ij} (P_1/d\phi)_{ij} (P_2/dr)_{ij} (P_3)_{ij} (P_4)_{ij} \qquad (4.1\text{-}17)$$

$$\bar{y} = \frac{\Delta r \Delta \phi}{R} \sum_i \sum_j y_{ij} (P_1/d\phi)_{ij} (P_2/dr)_{ij} (P_3)_{ij} (P_4)_{ij} \qquad (4.1\text{-}18)$$

$$\bar{E} = \frac{\Delta r \Delta \phi}{R} \sum_i \sum_j E_{ij} (P_1/d\phi)_{ij} (P_2/dr)_{ij} (P_3)_{ij} (P_4)_{ij} \qquad (4.1\text{-}19)$$

These calculated first moments should be indicative of the effective center of interaction in the atmosphere and the effective energy being detected.

The major assumption made in the derivation of this model is that only the single scattering of gamma rays is considered. In the present case this appears to be justifiable on the basis that the number of relaxation lengths encountered in the gamma-ray transport is small and the "geometry factors" are "good." We predict that 99% of all the initial gamma-ray interactions that contribute to the response of the gauge occur within 10 meters of the detector. At a density of 0.00129 g/cm^3 the number of relaxation lengths for a 0.100 Mev gamma ray at a distance of 10 meters is 0.20. Assuming that the slope of the buildup factor versus relaxation length for a

0.1 Mev gamma ray in air is as much as 2, the maximum error introduced at this extreme distance by multiple-scattering events is about 40%. Since the bulk of the scattering occurs at distances much smaller than this, we estimate that the maximum total error introduced by this assumption is less than 1%.

A secondary assumption was that the total efficiency and photofraction of the detector crystal was equal to that exhibited by a 2" x 2" cylindrical NaI(Tl) crystal with the source at an infinite distance away and placed on the cylindrical axis of the detector. Although this assumption seems like an oversimplification, it should be pointed out that the first moment about the source of all the gamma-ray interactions occurs at distances on the order of 1 meter as is shown later. This means that most of the gamma rays will intercept the surface of the cylindrical 2" x 4" detector almost perpendicularly. The major effect of this assumption and the previous assumption of single scattering should be to make the absolute values of the predictions questionable. The accuracy of the model to predict relative responses (e.g. responses for different source energies, source-to-detector distances, and various atmospheric compositions) should not be seriously affected.

The detailed equations for cross sections used in deriving this model can be found in standard texts such as that by Evans[1]. The computer program of this model was written in FORTRAN II and run on the Bunker-Ramo 340 digital computer. A calculation of the response for one set of conditions takes about 15 minutes of computation time.

4.2 Modification of Model for Calibration Sphere Scattering

The prototype gauges to date have been calibrated in a steel sphere with a diameter of 60 feet. This has been accomplished by placing the rocket containing the gauge in the center of the steel sphere and obtaining gauge responses to various known atmospheric densities in the sphere. A large amount of scattering from the sphere walls was noticed in these calibrations, but it was assumed to be constant and independent of the atmospheric density inside the sphere. The gauge calibration

was taken as the response to various atmospheric densities minus the response at zero density in the sphere.

It occurred to us that the amount of scattering from the sphere walls is not likely to be independent of the density inside the sphere, since the amount of wall scattering will be attenuated and rescattered by the atmosphere inside the sphere. This would affect the true slope of the calibration. Also the true background counting rate is indeterminate in this procedure. This means that the existing technique of calibration does not give an accurate calibration for the case of interest: viz. when the rocket and gauge are in an infinite homogeneous atmosphere. In the hope of correcting this calibration procedure we decided to derive a model which would predict the number of gamma rays that are scattered by a spherical steel wall into the gauge when it is located at the center of the steel sphere. The response of the gauge due to scattering in the atmosphere before reaching the steel wall can be calculated with the basic model described in Sec. 4.1 integrated out to the radius of the sphere.

Since one can only count on the relative accuracy of these models, a technique for using the two models to predict the true gauge calibration must be derived which does not require direct additions of the predictions from each model. Assuming that the prediction of the model described in this section is denoted M_2 and the prediction of the model described in Sec. 4.1 is denoted M_1, then the response inside a steel sphere is given by:

$$R_s = K_1 + K_2 M_1 + K_3 M_2 \qquad (4.2\text{-}1)$$

where K_1 = the true background counting rate due to multiple scattering through the shield, natural radioactivity in the rocket, electronic noise, and cosmic rays; a constant,

M_1 = model prediction of atmosphere scattering integrated to the sphere radius,

M_2 = model prediction of wall scattering from the sphere,

K_2 and K_3 = constants.

By using experimental data from two spheres of different diameters with the appropriate model predictions, one can determine the 3 constants of Eq. (4.2-1) by a least-squares method. The true response in an infinite atmosphere which serves as the corrected calibration can be predicted from:

$$R_a = K_1 + K_2 M_1 \qquad (4.2\text{-}2)$$

where M_1 is the model of atmosphere scattering integrated to infinity rather than to the sphere radius.

The model for determining the amount of scattering from the calibration sphere walls was derived by assuming that a point source of gamma rays at a distance equal to the sphere radius from a spherical detector is representative of the total wall scattering. The point source is anisotropic; the number of gamma rays emitted at any angle from the line connecting the source and detector is determined by assuming that the original gamma ray of chosen energy was emitted from the sphere center and scatters back at various probabilities at each angle and energy according to the Compton scattering cross section given by:

$$\frac{d\sigma_e(\theta)}{d\theta} = \pi r_o^2 \sin\theta \, (h\nu'/h\nu_o)^2 \, (h\nu'/h\nu_o + h\nu_o/h\nu' - \sin^2\theta) \text{ cm}^2/\text{electron} \qquad (4.2\text{-}3)$$

where $\frac{d\sigma_e(\theta)}{d\theta}$ = the fractional number of gamma rays in a beam with energy $h\nu_o$ and direction $\theta = 0°$ that are scattered at the angle θ per electron/cm^2/differential angle.

If the coordinate origin is shifted to the point source on the wall with the 0° line being that from the source to the detector, then it is seen that the

angular distribution of the source is proportional to $-d\sigma_e(\pi - \theta)$.

$$D(\theta) = Cd\sigma_e(\pi - \theta) \sum_i w_i Z_i / A_i \qquad (4.2\text{-}4)$$

where $D(\theta)$ = the fractional number of gamma rays with energy $h\nu'$ and direction θ within the differential angle $d\theta$,

and C = the effective scattering density thickness of the steel wall for the original gamma-ray energy $h\nu_o$, in g/cm^2.

The effective scattering density thickness was taken as:

$$C = A\, E^n \qquad (4.2\text{-}5)$$

where A and n are constants determined from the points E = 1.25 Mev, $C = 14.9\ g/cm^2$ and E = .135 Mev, $C = 1.57\ g/cm^2$.

The finite-difference form of Eq. (4.2-4) is:

$$D(\theta_a) = -C(\theta_1 - \theta_2) \frac{d\sigma_e(\pi - \theta_a)}{d\theta} \sum_i w_i Z_i / A_i \qquad (4.2\text{-}6)$$

where $\theta_a = (\theta_1 + \theta_2)/2$.

Number albedoes could be substituted directly for $D(\theta)$, but unfortunately none were found in the literature for steel.

Fortunately, this model is again cylindrically symmetrical about the line from the wall point source to the detector. The model can be set up identically to the basic model described in Sec. 4.1 with the exceptions that: (1) the source is anisotropic, (2) the minimum scattering angle is defined by the line from the point source that is tangent to the detector surface while the maximum angle is $\pi/2$, (3) the detector is spherical in shape, (4) the model is integrated to the steel sphere radius, and (5) a simple direct transmission calculation to account for gamma rays scattered directly back at the detector must be added to the model response.

Only those gamma rays are included in the model that are scattered once from the atmosphere inside the sphere or the sphere wall after the original scatter at the wall. The justifications for using only single scatters in this case are the same as for the basic model described in Sec. 4.1.

The assumption that the total wall scattering can be represented by the scattering from one point on the wall surface to a spherical detector is not as stringent as it may appear at first look. Since 99.9% of the interaction volume is farther than 1 meter from the detector, the orientation of the detector becomes relatively unimportant. Also, even though the scattering from different points on the wall may give rise to different absolute responses due to the orientation of the rocket and gauge, the relative change in this response with changes in atmospheric density inside the sphere should remain essentially constant from one point to another. Since only relative predictions are required for the ultimate use of the model predictions in Eq. (4.2-1), the assumptions are justifiable.

The computer program of this model was written in FORTRAN II and run on the Bunker-Ramo 340 digital computer. A calculation of the response for one set of conditions takes about 10 minutes of computation time.

4.3 Model Modified for Rocket Wall Streaming

One of the limitations on the accuracy of the prototype gauges has been an unexplained high background counting rate (counting rate at zero atmospheric density) of about 500 to 1700 counts per second. If this background could be reduced significantly, much lower densities could be measured. It occurred to us that one source of background counts could be the streaming of gamma rays down the outer shell of the rocket wall and then into the detector. To evaluate this effect, the basic model described in Sec. 1.1 has been modified to include initial scattering down the wall and subsequent scattering from the wall into the detector.

The significant changes in the model described in Sec. 4.1 are: (1) the

P_1 probability given by Eq. (4.1-1) does not include an attenuation term since the integration on r is only done to the outer surface of the rocket wall, (2) the P_2 probability given by Eq. (4.1-9) substitutes a term for $\frac{d_x}{2\pi S_x}$ that describes the fractional amount of the solid angle between θ_1 and θ_2 that is intercepted by the circular rocket wall, (3) the P_3 probability is the exponential attenuation of the wall from the original scattering point in the wall at r and ϕ to a point in the wall adjacent to the leading edge of the detector, and (4) the P_4 probability includes the probabilities that each gamma ray reaching the point adjacent to the leading edge of the detector is not attenuated further as it progresses down the wall, that it is scattered from a point within the wall to intercept the detector, and that the detector will detect the intercepted gamma ray at the second scatter energy. The P_4 probability is the most complicated in this model since 10 scattering points within the rocket wall are calculated for each of 10 positions on the detector. Therefore 100 separate calculations are necessary for each P_4 value.

The major assumption made in deriving this model is that all scattering that occurs in the wall after the initial scatter results in the removal of gamma rays from the beam that are "streaming" down the wall. It is obvious that some of these scattering events that result in very small direction changes do not remove gamma rays from the beam. The result of this assumption is to cause the model to predict a minimum of background counts due to this effect.

The computer program of this model was written in FORTRAN II and run on the Bunker-Ramo 340. A calculation of the response for one set of conditions takes about 12 minutes of computation time.

4.4 Monte Carlo Calculation of Shield Effectiveness

Another possible source of high background counting rates is the penetration of gamma rays through the conical tungsten shield placed between the source and detector. To evaluate this effect we decided to use an existing Monte Carlo method

for calculating deep gamma-ray penetration derived by Chilton[3]. This method uses an exponential transformation to optimize the number of random walks necessary to obtain a given accuracy.

One major assumption that was made in using this method was that the shield used in the calculation has infinite dimensions in the directions normal to the axis of the source and detector rather than the actual conical dimensions. This assumption tends to make the predicted amount of penetration higher than actual since gamma rays scattered normally to the source-detector axis could be scattered back toward the detector from the assumed shield configuration. This would not occur past the true dimensions of the shield.

Another major assumption was that the source was distributed evenly over the back surface of the shield and all gamma rays emitted from this source were perpendicular to the shield surface. This assumption is not too restrictive since the actual angle between a line perpendicular to the back surface of the shield and the line connecting the source to the shield extremity does not vary from 90° by more than 6°.

The computer program of this calculation method was written in FORTRAN 64 and run on a CDC 3600 digital computer. A calculation of the gamma-ray penetration for one set of conditions takes about 30 minutes of computation time.

5. GENERAL MODEL PREDICTIONS

In this section the general predictions of the models are presented. The response to density is given first. Then the effects of variations in atmospheric composition variations in source energy and placement, variations in atmospheric density due to shock wave perturbations, and variation in rocket wall properties are treated. Unless otherwise discussed the dimensions used correspond to those of the prototype gauge mounted in an Apache rocket as given in NASA Drawing No. LR-806522. For convenience, dimensions of the pertinent items shown in Fig. 1 and used in the derivation of the model in Sec. 4.1 are given in Table 1. The rocket wall was assumed to be composed of 24% by weight of carbon and 76% by weight of fluorine and to have a density of 1.00 g/cm^3.

5.1 Response to Atmospheric Density

The response of the gamma-ray scatter gauge predicted by the model outlined in Sec. 4.1 is linear with density over the range from zero to atmospheric for source energies from 100 Kev to 2 Mev and source-to-detector distances from 12 inches to 30 inches. This was determined by calculating gauge responses with the model of Sec. 4.1 for various densities while holding all other variables such as atmospheric composition, source energy, and gauge configuration constant. A sample set of calculated results is given in Table 2. Note that the small deviation in linearity occurs as a decrease in response with increases in pressure. This is the result that one expects since in the extreme case of infinite density, the predicted gauge response should return to zero.

The result that the predicted gauge response is linear with atmospheric density allows one to significantly reduce the number of model calculations that are necessary in the study of the gamma-ray technique. The result obtained at one density is easily corrected to that at any density by multiplying by the ratio of the desired density to that used in the calculation.

To graphically illustrate how the gamma-ray scatter gauge works, a plot of the number of gamma rays scattered and eventually detected at any distance from the source and detector per 1000 detected gamma rays is shown in Fig. 3. The data for this plot was generated by the basic model described in Sec. 4.1 for a source energy of .134 Mev, the dimensions given in Table 1, a detector efficiency equal to the total efficiency of a 2" x 2" NaI(Tl) crystal, and an air density of .00100 g/cm^3. Note that the number of gamma rays eventually detected are maximum at a distance of about 40 cm and approach zero assymtotically as the distance considered is increased.

5.2 Response to Variation in Atmospheric Composition as a Function of Source Energy

Since it is known that the composition of the atmosphere varies slightly with altitude and also the densities of atmospheres other than that of the Earth (such as that of Mars) may be desired, the effect of atmospheric composition variations was studied by using the model described in Sec. 4.1. The NASA Model IV atmosphere of Mars[4] was compared to that of the Earth by inserting each composition into the model of Sec. 4.1 at the same atmospheric density. The composition of Mars assumed by NASA Model IV and the standard composition of Earth are given in Table 3. The predicted gauge responses for these two compositions for various gamma-ray energies are given in Table 4 and plotted in Fig. 4.

At gamma-ray energies greater than 0.134 Mev, the only difference between the predicted responses to the two atmospheric compositions (0.970) is that due to the difference in the effective ratio of the atomic number of atomic weight. The electron density, which is part of the Compton scattering cross section, depends directly on this ratio. Except for hydrogen, most other gaseous elements have a ratio of atomic number to atomic weight that is essentially constant and equal to 0.5. The error introduced by the difference in this ratio is only about 3% for the present case and is due primarily to the presence of argon. The response error

increases rapidly at gamma-ray energies lower than 0.080 Mev due to the increased dependence of the gauge response on the photoelectric effect. This effect depends quite strongly on composition [see Eq. (4.1-6)]. The NASA Model IV of the Mars atmosphere was chosen to represent the maximum possible deviation from the atmosphere of the Earth or any other assumed composition for Mars due to the large value of the photoelectric effect exhibited by argon.

It can be seen from Fig. 4 that gamma-ray energies less than about .080 Mev ought to be avoided in using this principle for measuring atmospheric densities if the composition of the atmosphere varies or is an unknown quantity. This means that the gamma-ray energy which gives maximum sensitivity as indicated on Fig. 4 (.038 Mev for the atmosphere of the Earth and .056 Mev for the NASA Model IV atmosphere of Mars) cannot be used. Fortunately, the sensitivity at 0.100 Mev is still 80 to 90% of the maximum sensitivity and one could therefore use gamma-rays of about this energy without much loss in sensitivity.

5.3 Response to Variations in Source Energy and Source-to-Detector Distance

The predicted response of the gauge to variations in source energy for air at sea level is shown in Fig. 4. The first moments of the horizontal distance and vertical distance about the source are given in Table 5. These parameters were calculated according to Eqs. (4.1-17) and (4.1-18). Examination of these data show that the effective center of interaction changes very slowly as the gamma-ray energy decreases from 2.2 Mev to .03 Mev. Only energy decreases beyond .03 Mev begin to cause a significant reduction in the distance from the rocket center line to the effective interaction point. It is important to note that the effective interaction point is about 1 meter from the rocket center line over this wide range of source energies. This indicates that the effective sample volume is always quite large and that the distance to the interaction point and back to the detector controls the response by the inverse square law more strongly than it does by attenuation of the gamma rays.

The effect of varying the source-to-detector distance is shown in Table 6 for the three gamma-ray energies 0.134, 0.694, and 2.180 Mev. Note that the response change with source-to-detector distance is very slight in the range from 30 to 60 cm. This is to be expected from the fact that the effective center of the gamma-ray interactions is about 100 cm from the rocket center line. The distance between source and detector is small compared to the total path length of the average gamma ray that is scattered by the atmosphere and subsequently detected. The effect of source-to-detector distance on the gauge response to atmospheric density is therefore small. On plotting the data of Table 6 it is found that the gauge response is directly proportional to the reciprocal of the source-to-detector distance.

5.4 Response to Density Variations Induced by Shock Waves

The response of the gamma-ray scatter gauge to shock wave density perturbations was determined by introducing into the basic model a conical shock wave around the rocket. The shock wave was assumed to be delineated sharply by a conical surface with origin at the front of the rocket nose. Any angle between the rocket axis and the shock wave interface could be assumed. The density inside the conical shock wave was assumed to be homogeneous and was taken as the arithmetic average value of the density at the shock wave interface and at the vehicle surface. Shock wave angles and density ratios were taken from Refs. 5 and 6.

Sample results of the calculated predictions are given in Table 7 for a gamma-ray source energy of 0.134 Mev. Results are shown for the composition of the atmosphere of Earth and for the NASA Model IV composition of Mars at the density of air at sea level for a range of Mach numbers from 1 to 4.6. It is obvious from these results that the effect of realistic shock wave density perturbations are negligible since the maximum error introduced is 1.9%. Other gamma-ray source energies were used in similar calculations and showed no significant difference at

energies between 50 Kev and 2.2 Mev. Source-to-detector distances from 12 to 24 inches were also used in the calculation and also showed no significant difference. When atmospheric densities less than that at sea level were used in the calculation, the shock wave density perturbations predicted lesser effects than those shown in Table 7.

The fact that shock wave density perturbations do not significantly affect the gauge response can be explained by noting the previously reported result that the effective center of interaction in the atmosphere is about 1 meter from the rocket. This means that on the average each detected gamma ray must travel 2 meters (to the interaction point and back) before it is detected. The distance traveled through the shock wave is therefore negligible compared to the total effective path length of the average gamma ray.

5.5 Response to Container Properties

The background counting rate due to the streaming of gamma rays down the rocket wall with subsequent scattering into the detector was calculated for various source-to-detector distances within the Apache rocket and for three source energies by using the model described in Sec. 4.3. The results of these calculations are listed in Table 8 and plotted in Fig. 5. The gauge response to atmospheric density for a source energy of 0.134 Mev as calculated by the basic model is also plotted on Fig. 5 for sake of comparison. The detector efficiency subroutine was used in these calculations with a lower discriminator setting of 90 Kev, an upper discriminator setting of 155 Kev, and a standard deviation of the detector pulse-height spectrum of 4.24%. Under these conditions the basic model predicts that the gauge response to source energies of 0.694 and 2.180 Mev are less than that at 0.134 Mev by a factor of 100.

The importance of these results is that the background counting rate due to gamma-ray streaming down the rocket wall depends very strongly on the source-

to-detector distance while the response to atmospheric density is only a very weak function of this distance in the range of interest. A change of 30 cm in the source-to-detector distance reduces the amount of gamma-ray streaming by a factor of 293 while the response to atmospheric density is decreased by only a factor of 2.13. It is evident from this that a small increase in the source-to-detector distance could show great improvement in the signal-to-noise ratio of the gauge.

6. SPECIFIC MODEL PREDICTIONS

In this section some specific predictions are made about the gamma-ray scattering principle in an effort to explain certain data taken with the prototype gauges. The response to the three major gamma-ray energies of ^{144}Ce under the specific counting conditions used are treated first. Then the shield effectiveness for the most energetic gamma ray (2.180 Mev) of ^{144}Ce is predicted for the same counting conditions. Finally, the correction technique for calibration is discussed and the response of the gauge with the movable shield closed is compared to the response with the shield open.

The specific counting conditions chosen are: (1) a lower discriminator setting of 80 Kev, (2) an upper discriminator setting of 150 Kev, and (3) a detector pulse-height standard deviation of 4.24%. The total efficiency E_t and photofraction F_p were taken as those for a point source on the axis of a cylindrical 2" x 2" NaI(Tl) crystal at an infinite distance. Data at various gamma-ray energies were taken from Crouthamel[2] and used to fit a fourth-order polynomial for both E_t and F_p. The specific efficiency as a function of incident gamma-ray energy for these counting conditions is plotted in Fig. 6. The total efficiency for all pulses is also plotted in Fig. 6 for comparison.

6.1 Response to Gamma-Ray Energies of ^{144}Ce - ^{144}Pr

The response of the gauge to the three major gamma-ray energies of ^{144}Ce - ^{144}Pr above 80 Kev were calculated for the specific counting conditions used in the prototype gauge. The results of these calculations are given in Table 9. As might be expected from the predicted counting efficiencies given in Fig. 6, the response of the gauge to the 0.694 and 2.180 Mev gamma rays is negligible compared to the response to the 0.134 Mev gamma ray.

A comparison of the predicted gauge response to that obtained with the prototype can be made with this data. According to Hakewessel[7], the gauge

response to a 21.4-curie source of ^{144}Ce - ^{144}Pr for a 2" x 4" NaI(Tl) cylindrical detector cut in half along the axis with discriminator settings of 90 and 155 Kev was 315,000 pulses per second. This value was obtained by extrapolating the results given in Fig. 38 of Ref. 7. The value predicted by the basic model would be:

$$\left[.1552 \times 10^{-5} \frac{\text{pulses/second}}{\text{disintegrations/second}}\right] \left[21.4 \text{ curies}\right] \left[3.7 \times 10^{10} \frac{\text{disintegrations}}{\text{curie-second}}\right] \frac{1}{2} =$$

$$614{,}400 \text{ pulses/second} \qquad (6.1\text{-}1)$$

This value is 95% higher than actual, which is a reasonable agreement of absolute values considering the accuracy to which the source strength could be ascertained and the fact that the effect of source self-absorption was not accounted for. The relative accuracy of the model prediction should be as much as an order of magnitude better than this.

6.2 Shielding Effectiveness

The background counting rate due to the penetration of gamma rays through the 9.5" conical tungsten shield was predicted for the prototype gauge by the method outlined in Sec. 4.4. Only 2.180 Mev gamma rays were considered since this energy should penetrate thick shields of this type by considerably more than energies lower than 0.7 Mev. The predicted response per unit disintegration of ^{144}Ce - ^{144}Pr was $.382 \times 10^{-11}$. For a 21.4-curie source of ^{144}Ce - ^{144}Pr detected by half of a 2" x 4" cylindrical detector with discriminator settings as before, the predicted background counting rate is:

$$\left[.382 \times 10^{-11} \frac{\text{pulses/second}}{\text{disintegrations/second}}\right] \left[21.4 \text{ curies}\right] \left[3.7 \times 10^{10} \frac{\text{disintegrations}}{\text{curie-second}}\right] \left(\frac{1}{2}\right) =$$

$$15.2 \text{ pulses/second} \qquad (6.2\text{-}1)$$

This predicted background counting rate represents 3.6% of the 440 pulses/second reported by Hakewessel[7] and therefore is negligible.

The background counting rate due to the penetration of gamma rays through the source shield, R_{bs}, depends on the inverse square of the source-to-detector distance.

$$R_{bs} = \frac{2.77 \times 10^6}{d^2} \qquad (6.2\text{-}2)$$

An increase in the source-to-detector distance of 10 cm without a change of shield size, decreases the background counting rate due to the penetration of gamma rays through the shield by a factor of 0.65.

6.3 Background Counting Rate Due to Gamma-Ray Wall Streaming

Using the data given in Table 8 and discussed in Sec. 5.5, the absolute value of the background counting rate due to gamma-ray wall streaming can be calculated and compared to the total background counting rate obtained on the prototype gauge[7]. The background counting rate obtained for a 21.4-curie source of ^{144}Ce - ^{144}Pr with half of a 2" x 4" cylindrical NaI(Tl) crystal operated with discriminator settings of 90 and 155 Kev was 440 pulses/second. Using the predicted responses per unit gamma ray of energies of 0.134, 0.694, and 2.180 Mev at the 42.23 cm source-to-detector distance given in Table 8 with the gamma-ray abundances given in Table 9, the gamma-ray streaming pulse rate per unit disintegration rate is found to be:

$$(.300)(.1897 \times 10^{-8}) + (.020)(.03725 \times 10^{-8}) + (.030)(.02694 \times 10^{-8}) =$$

$$.5846 \times 10^{-9} \frac{\text{pulses/second}}{\text{disintegrations/second}} \qquad (6.3\text{-}1)$$

From this value one can calculate the background counting rate due to gamma-ray wall streaming for the prototype gauge.

$$R_{bss} = \left[.5846 \times 10^{-9} \frac{\text{pulses/second}}{\text{disintegrations/second}} \right] \left[21.4 \text{ curies} \right] \left[3.7 \times 10^{10} \frac{\text{disintegrations}}{\text{curie-second}} \right] \quad (\tfrac{1}{2})$$

$$= 231 \text{ pulses/second} \qquad (6.3\text{-}2)$$

This represents 53% of the actual total background counting rate. Since this is a minimum estimate (see Sec. 5.5), it is obvious that gamma-ray streaming represents a major fraction of the background counting rate. Small changes in the source-to-detector distance would significantly decrease the amount of background due to this effect. From Table 8 it is found that an increase from 42.23 cm to 60.96 cm would decrease the amount of background by a factor of 29.3 or to 7.9 pulses/second. The signal-to-noise ratio would be altered by a factor of 19.7 if the background is considered to be solely due to streaming.

6.4 Correction Procedure for Sphere Calibration

The model described in Sec. 4.2 was used to predict the prototype gauge response inside two calibration spheres. The relative responses of each model for steel calibration spheres with diameters of 60 and 41 feet are given in Table 10 and plotted in Fig. 7. These data can be used with the data of Hakewessell[8] for a 60 foot steel sphere to predict the constants K_2 and K_3 of Eq. (4.2-1) when K_1 is assumed to be zero. The pertinent prototype data is R_s = 890 pulses/second when ρ = .0005 g/cm^3 and R_s = 310 pulses/second when ρ = 0 g/cm^3. The relative model values for these two cases are M_1 = 0 and M_2 = 1 when ρ = 0 g/cm^3, and M_1 = 1 and M_2 = 1.077 when ρ = .0005 g/cm^3. Substituting these values into Eq. (4.2-1) gives two equations which can be solved simultaneously to give a value of K_2 = 556.13 and K_3 = 310.

When the density term is substituted into the M_1 term the corrected calibration would be given by:

$$R_a = 1{,}112{,}200\ \rho \qquad (6.4\text{-}1)$$

The previous calibration technique would give:

$$R_a = 1{,}160{,}000\ \rho \qquad (6.4\text{-}2)$$

This difference represents an error of about 4.1%.

6.5 Movable Shield Response

One puzzling data anomaly observed on a prototype gauge occurred when a small tungsten cup was used to attenuate the ^{144}Ce - ^{144}Pr source in one-second cycles. The counting rate with each detector was found to be reduced by only a factor of two for air at sea level when the source was attenuated by the tungsten cup. The counting rates at essentially zero air density were reversed; that is the counting rates of the detectors with the attenuator cup over the source was slightly higher than when the source was exposed.

We attempted a quantitative prediction of the counting rates for these two conditions, but were thwarted by the unavailability of either experimental data or an accurate theory for predicting the bremsstrahlung spectra produced by the beta particles emitted by ^{144}Ce - ^{144}Pr. Since such spectra form an integral part of an analysis of this type, we felt that a quantitative prediction would be seriously limited in accuracy. We therefore offer a qualitative explanation of this anomaly.

With the movable shield open the response to the atmosphere is due solely to the 0.134 Mev gamma rays from the ^{144}Ce - ^{144}Pr source. A significant portion of the response at zero air density is due to the streaming of these 0.134 Mev gamma rays. With the movable shield closed essentially all of the 0.134 Mev gamma rays are completely absorbed. However, a considerable amount of bremsstrahlung is produced by the beta rays from the ^{144}Ce - ^{144}Pr source. Since there are about 6.7 beta rays emitted for every 0.134 Mev gamma ray, these beta rays have energies up to 3 Mev, and the amount of bremsstrahlung produced depends on the atomic number of the absorber (tungsten has a high atomic number), the amount of bremsstrahlung

could be quite large. The effective energy of the bremsstrahlung is probably higher than 0.134 Mev so that the sensitivity for measuring air density would be relatively low compared to that for 0.134 Mev gamma rays. This would require more than half as many bremsstrahlung photons to obtain half the response of the 0.134 Mev gamma rays. These same bremsstrahlung photons would be more efficiently detected relative to 0.134 Mev gamma rays after streaming down the rocket walls since they are scattered twice in this process and the energy is therefore degraded enough to be detected at the discriminator settings used. This could cause the response at zero density to be slightly higher with the movable shield closed.

Although this is a qualitative description, all of the assumptions are consistent with the previous model predictions.

7. DISCUSSION OF RESULTS AND CONCLUSIONS

This discussion of results and listing of conclusions naturally divides into the general aspects of the gamma-ray scattering technique, the rather specific aspects associated with explaining data from prototype gauges, and an evaluation of the mathematical modeling approach to the present and future atmospheric density gauging problems.

As to the general aspects of the technique our analysis shows: (1) the gauge response is linear with atmospheric density in the range of interest, (2) the maximum sensitivity for the density of air (at a source-to-detector distance of 42.23 cm) is obtained with a gamma-ray source energy of .038 Mev, (3) the gauge response to atmospheric composition becomes appreciable at gamma-ray energies less than 0.1 Mev, (4) the gauge response is a relatively weak function of source-to-detector distance in the range from 30 to 60 cm, (5) the effective interaction point of all gamma rays is about 1 meter from the rocket, (6) a significant number of gamma-ray interactions occur at distances up to 10 meters from the rocket, (7) the response to shock wave perturbations is negligible, and (8) the response to gamma-ray streaming down the rocket wall is a strong function of the source-to-detector distance.

In some cases experimental data could be used to check the models. The predicted linear response to density has been observed in the prototype gauges. In addition a predicted value of the gauge response to air at sea level was 95% higher than the reported experimental value. Furthermore, the predicted results are self consistent. For example, the predicted effective interaction point and large sample volume are consistent with the large amount of wall scattering observed in a sphere with a radius of 60 feet.

As to the specific predictions of the gauge our analyses gave: (1) a predicted response to air at sea level that was 95% higher than the experimental

result, (2) the response to gamma-ray energies from ^{144}Ce - ^{144}Pr other than 0.134 Mev was negligible, (3) the response of the gauge to gamma rays that penetrate the 9.5" tungsten shield is negligible, (4) the response of the gauge to gamma rays that stream down the rocket wall is significant, but could be reduced drastically by a slight increase in source-to-detector distance, (5) the existing sphere calibration technique is incorrect, but could be corrected by a technique involving the use of our models on data taken from two spheres of different sizes, and (6) the anomalous movable shield data can be explained qualitatively by considering the bremsstrahlung produced by the beta particles from the ^{144}Ce - ^{144}Pr source.

The usefulness of the models has been demonstrated here by predicting the general characteristics of the gamma-ray scattering technique and by explaining certain data anomalies that have been observed. The model predictions are consistent with experimental data in those cases in which they can be checked. The models predict that the significant problems are: (1) gamma-ray streaming down the rocket wall, (2) calibration inaccuracies, and (3) composition if gamma-ray energies less than 0.1 Mev are used. The models predict that shock-wave density perturbations and shield effectiveness are not significant problems.

The models derived and discussed here could have been used as subroutines in a large computer program to optimize the design of the prototype gauges. Various gamma-ray sources, discriminator settings, source-to-detector distances, rocket wall materials, and shield thickness could be chosen by a multivariable search routine to determine the optimum design on the basis of the maximum signal-to-noise ratio.

The proposed Mars Probe density gauge could be modeled by the same general techniques that have been used here. The major difference is that the configuration of the proposed Mars Probe gauge is not cylindrically symmetrical and therefore has one more degree of complexity. The present models could be done in two dimensions while the Models for the Mars Probe gauge would have to be done in

three dimensions. We feel that the present models could be modified for use in the Mars Probe gauge design without increasing the computation time more than about a factor of five. However, the complexity of these models would warrant programming them on a larger computer -- probably the IBM 360, Model 75. If all the models are used simultaneously to optimize the gauge design this step would be necessary even with the present models.

The Mars Probe gauge may offer several problems of greater magnitude than the existing prototype gauges. These include: (1) a larger background due to scattering inside the space vehicle, (2) more background due to increased gamma-ray streaming in the thicker space vehicle walls, and (3) a variable response due to ablation of the heat shield through which the gamma rays must pass. This last problem may warrant the use of a more sophisticated detection technique in which gamma rays of two energy ranges are detected simultaneously.

The problems identified in the present program and the additional problems likely to be encountered in the proposed Mars Probe gauge make it seem desirable to apply modeling techniques to the study, and possible the optimization of the design of the proposed Mars Probe Gauge. In addition, these models should prove useful in obtaining the most accurate values of density from telemetered counting rate data.

8. REFERENCES

(1) Evans, R. D., The Atomic Nucleus, Chaps. 24, 25, and 26, McGraw - Hill Book Company, Inc., New York, 1955.

(2) Crouthamel, C. E., Applied Gamma-Ray Spectrometry, Pergammon Press, New York, 1960.

(3) Chilton, A. B., Nuclear Science and Engineering, 24, 200 (1966).

(4) Levin, G. M., D. E. Evans, and V. Stevens, "NASA Engineering Models of the Mars Atmosphere for Entry Vehicle Design," NASA TN D-2525, November 1964.

(5) "Conical Flow Tables," NA-55-671.

(6) Sims, J. L., "Tables for Supersonic Flow Around Right Circular Cones at Zero Angle of Attack," NASA SP-3004, 1964.

(7) Hakewessel, D., "Feasibility Study for an X-ray Backscatter Air Density Sensor," p. 63 and p. 73, Report No. GCC ER-80157, April 8, 1964.

(8) Ibid., p. 47.

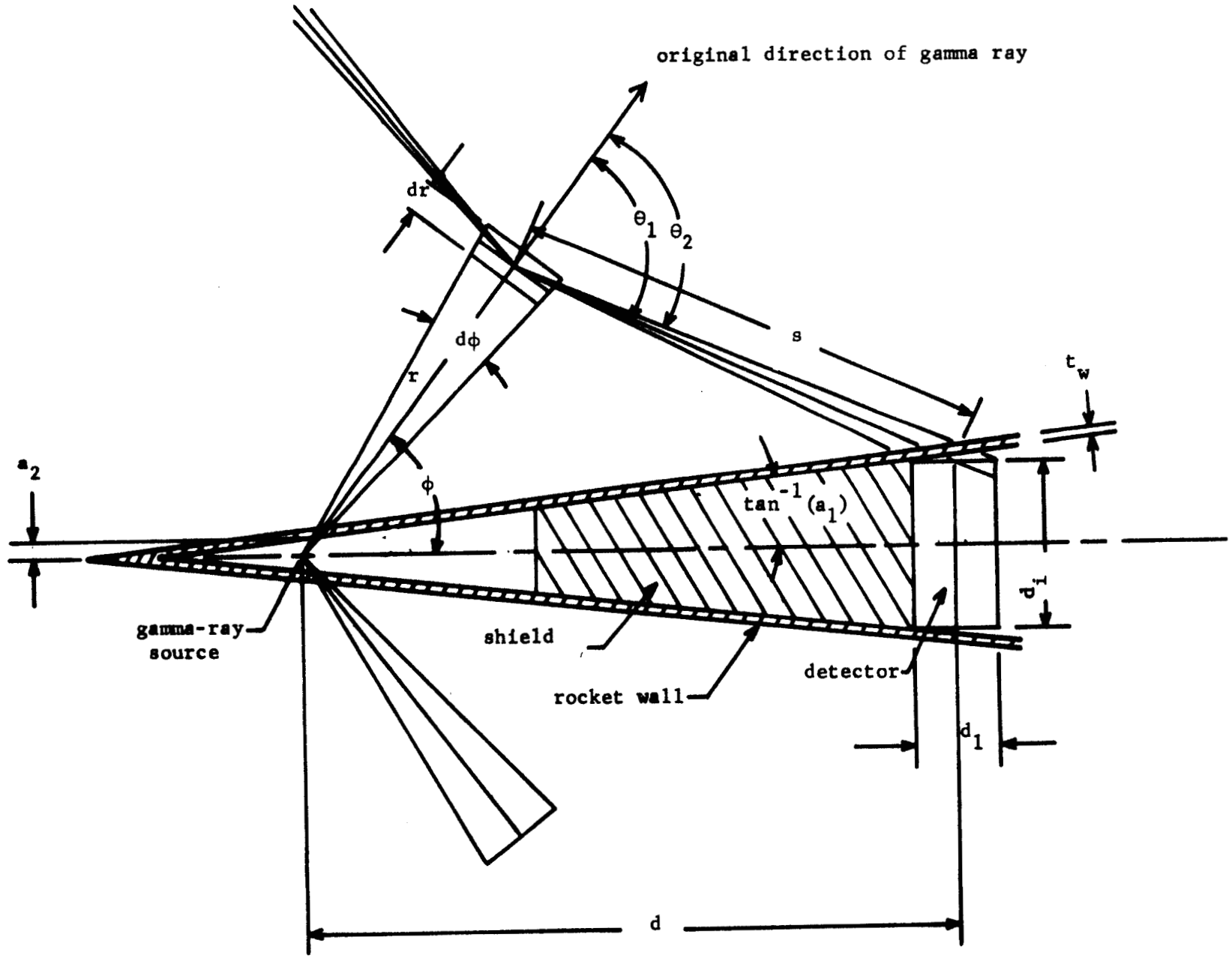

Fig. 1. Schematic drawing and coordinates of gamma-ray scattering system for measuring atmospheric density

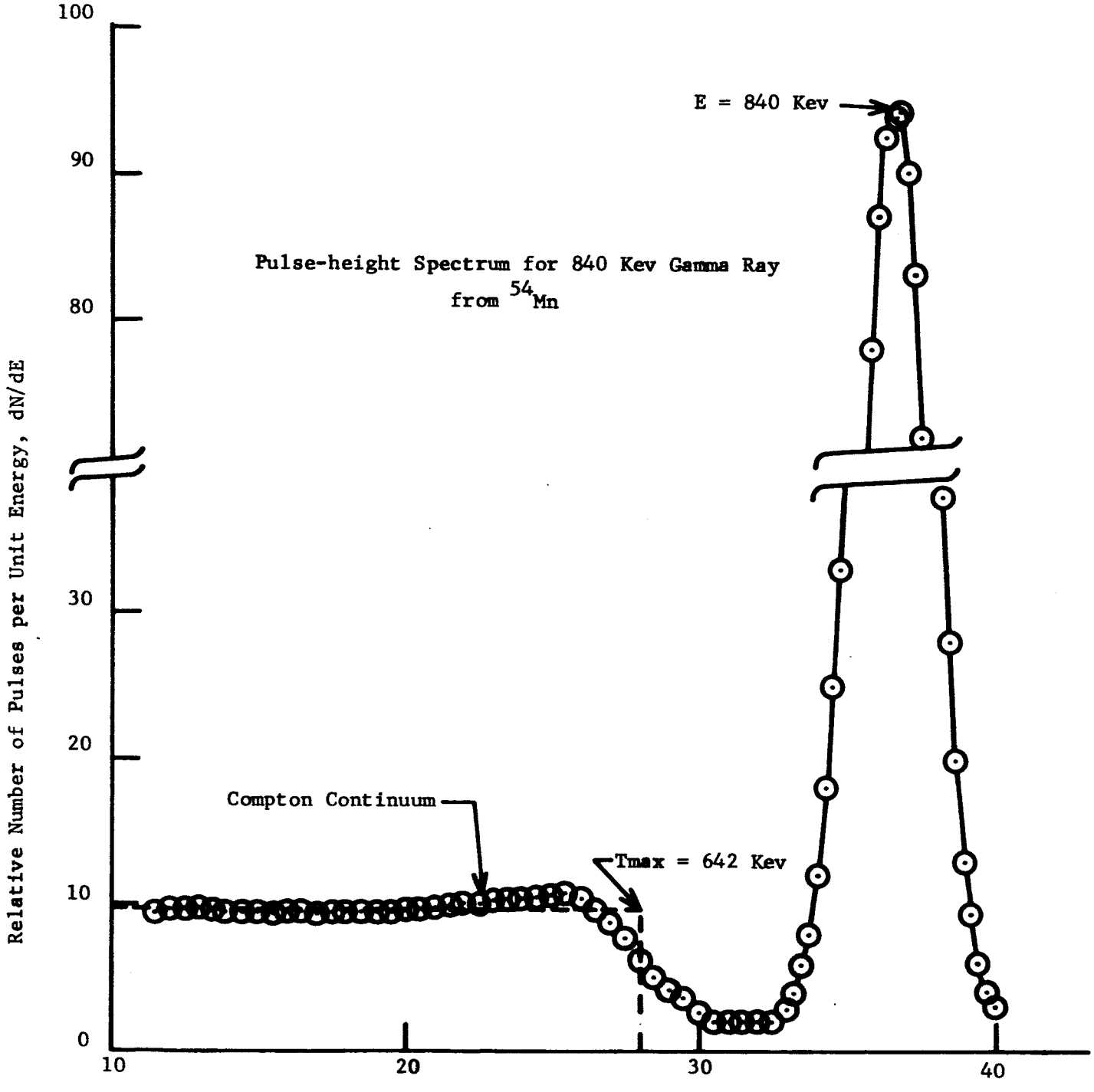

Fig. 2. Typical monoenergetic gamma-ray, pulse-height spectrum using a NaI(Tl) crystal and photomultiplier

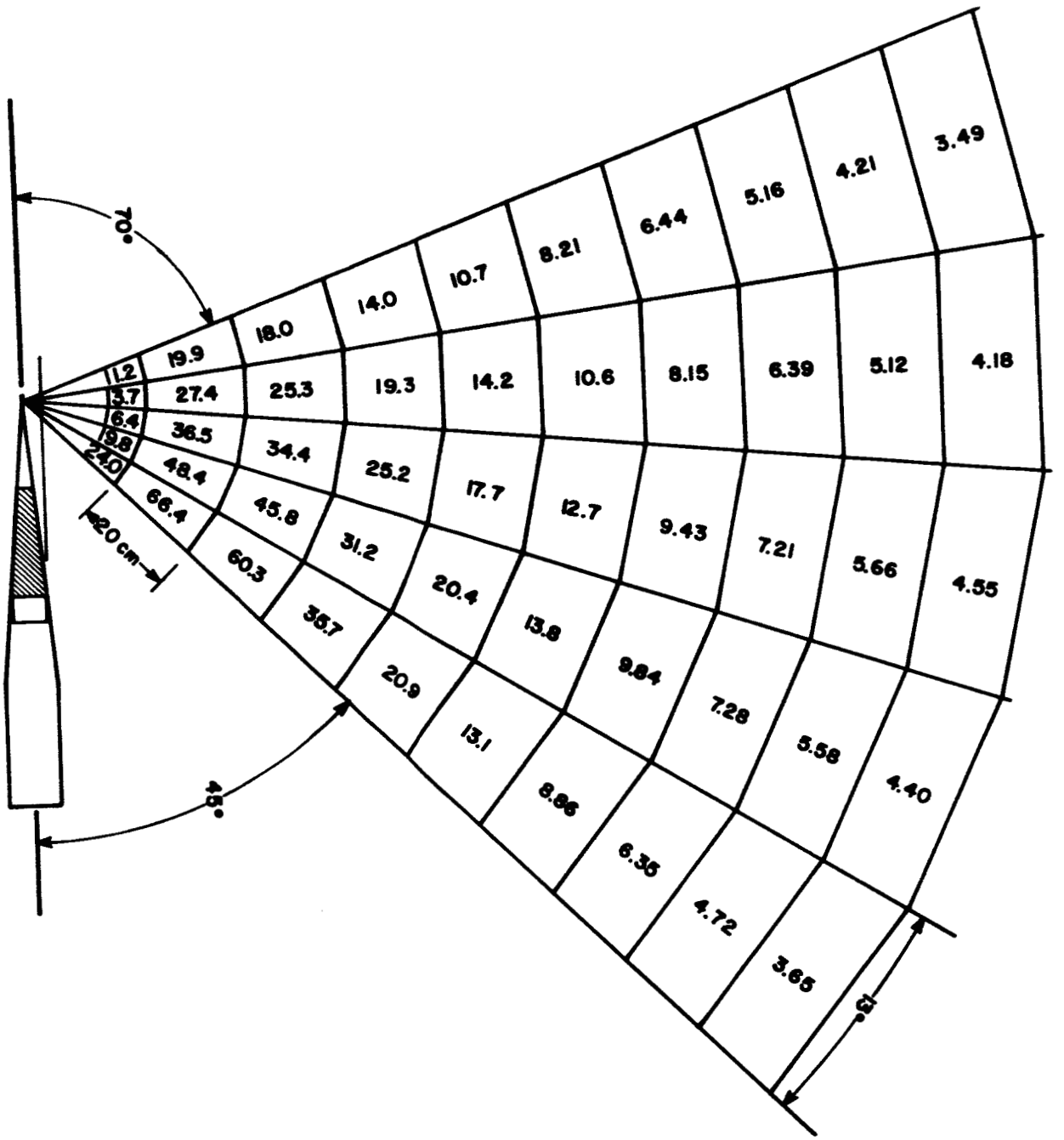

Fig. 3A. Predicted response per 1000 total units at various distances from rocket-mounted gauge

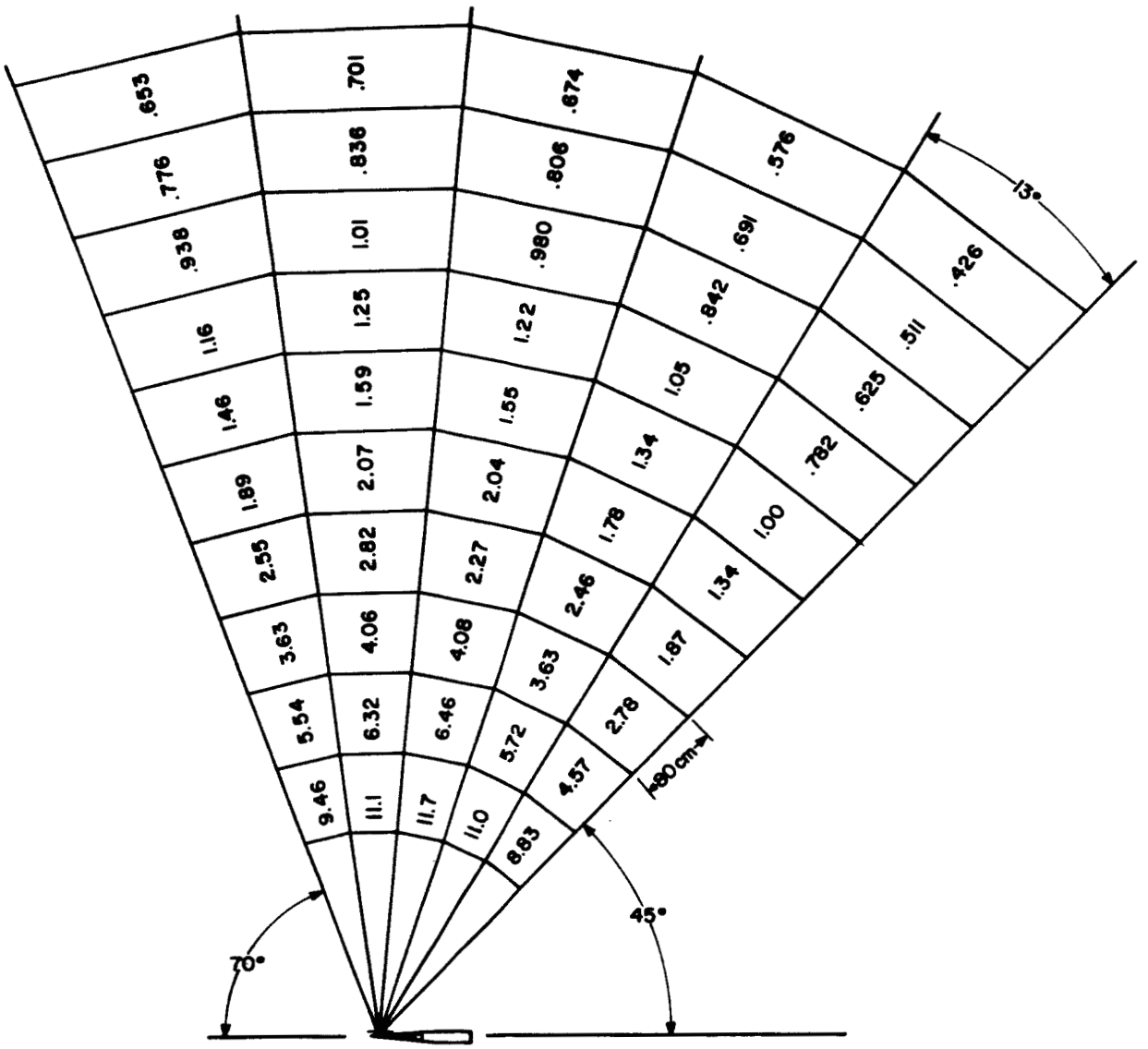

Fig. 3B. Predicted response per 1000 total units at various distances from rocket-mounted gauge

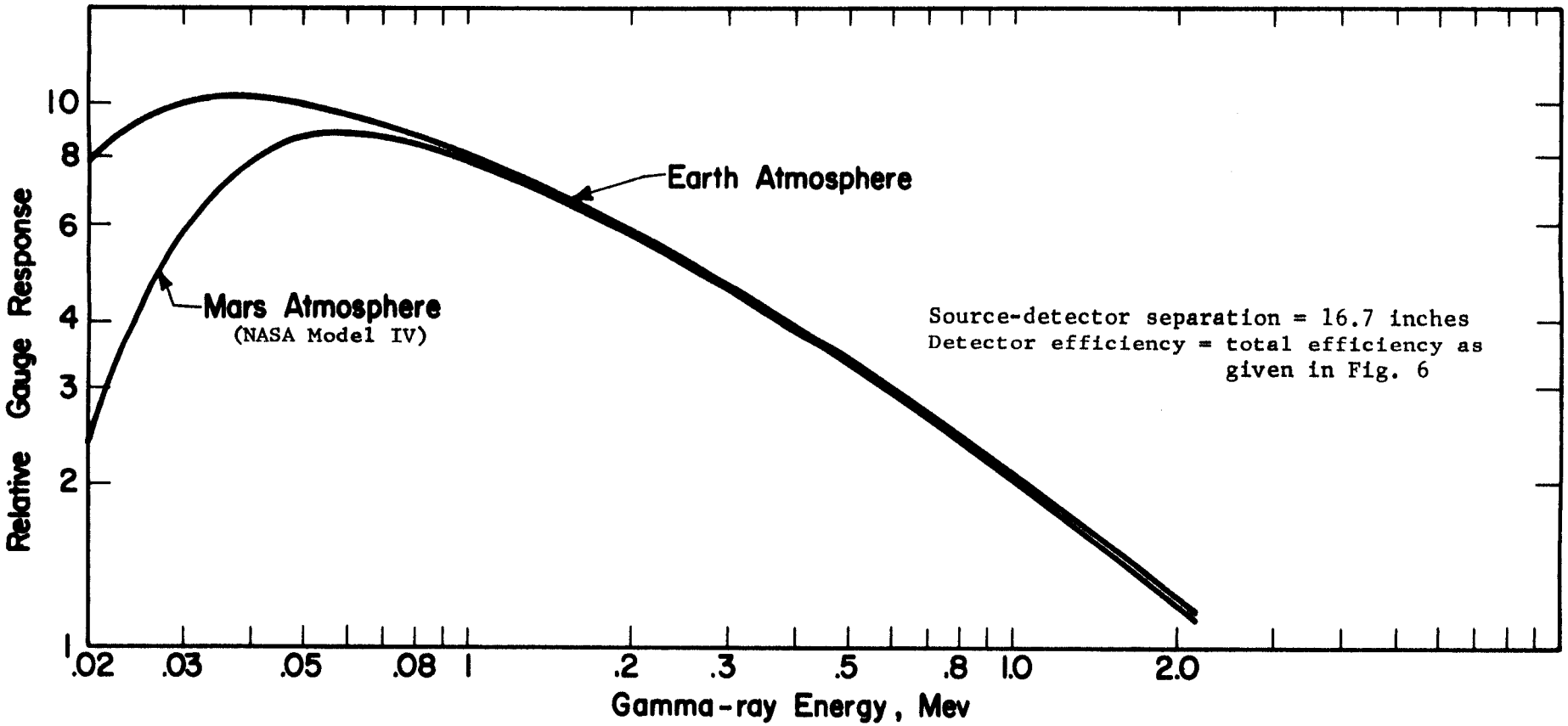

Fig. 4 Effect of gamma-ray source energy and atmospheric composition on predicted rocket-mounted, density gauge sensitivity

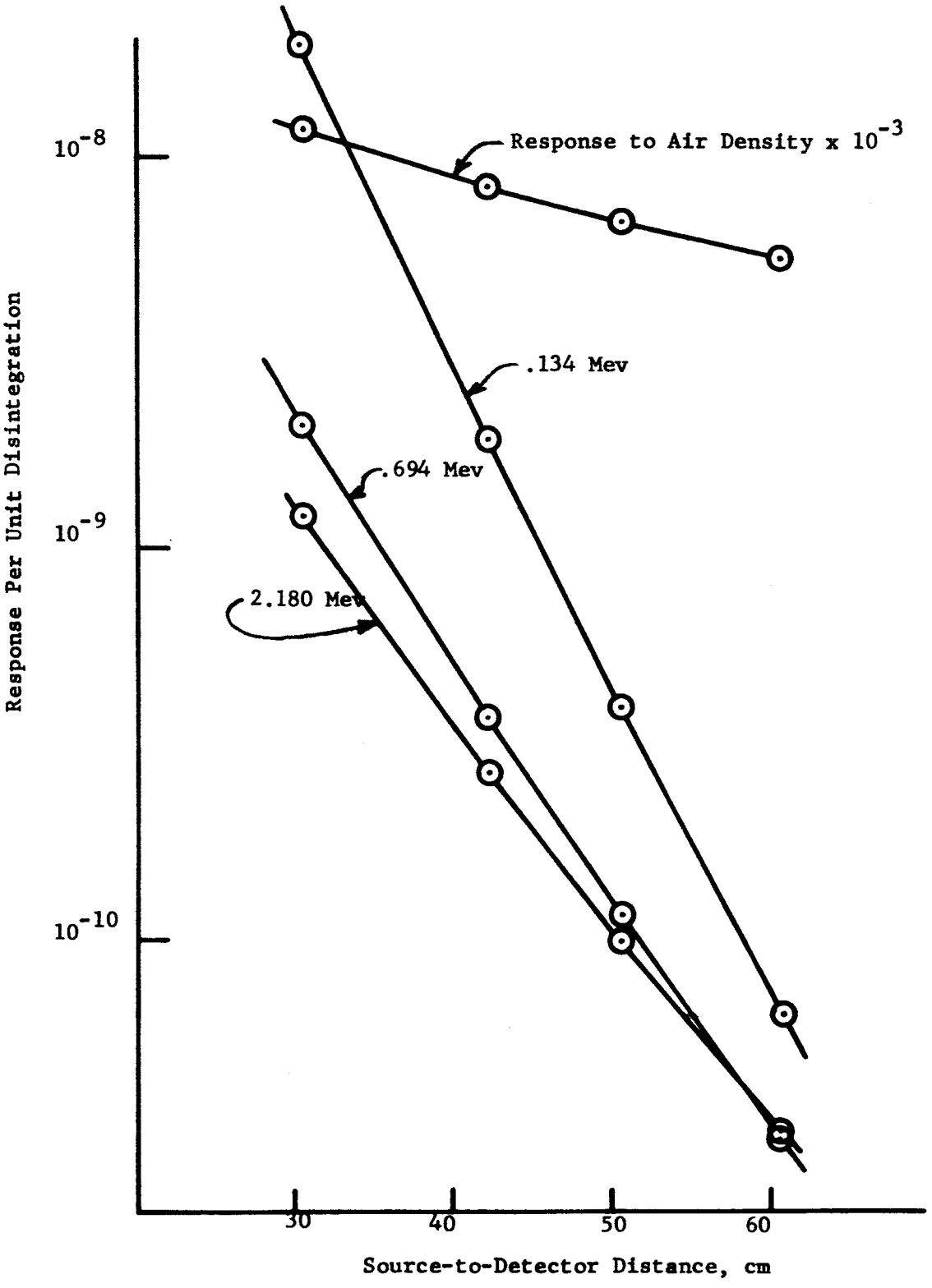

Fig. 5 Comparison of basic gauge sensitivity with gamma-ray wall streaming as a function of source-detector separation

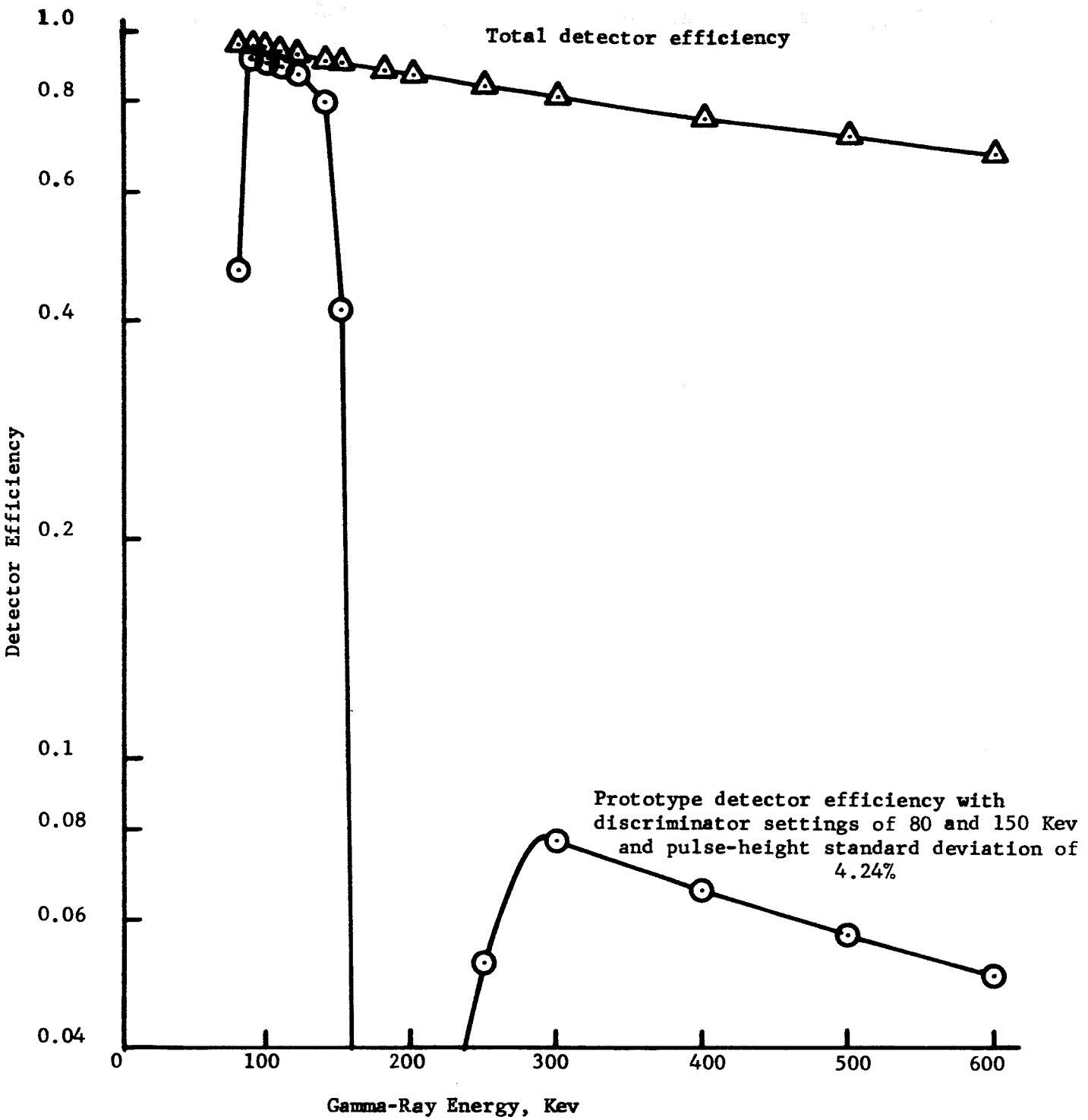

Fig. 6. Total and prototype detector efficiency

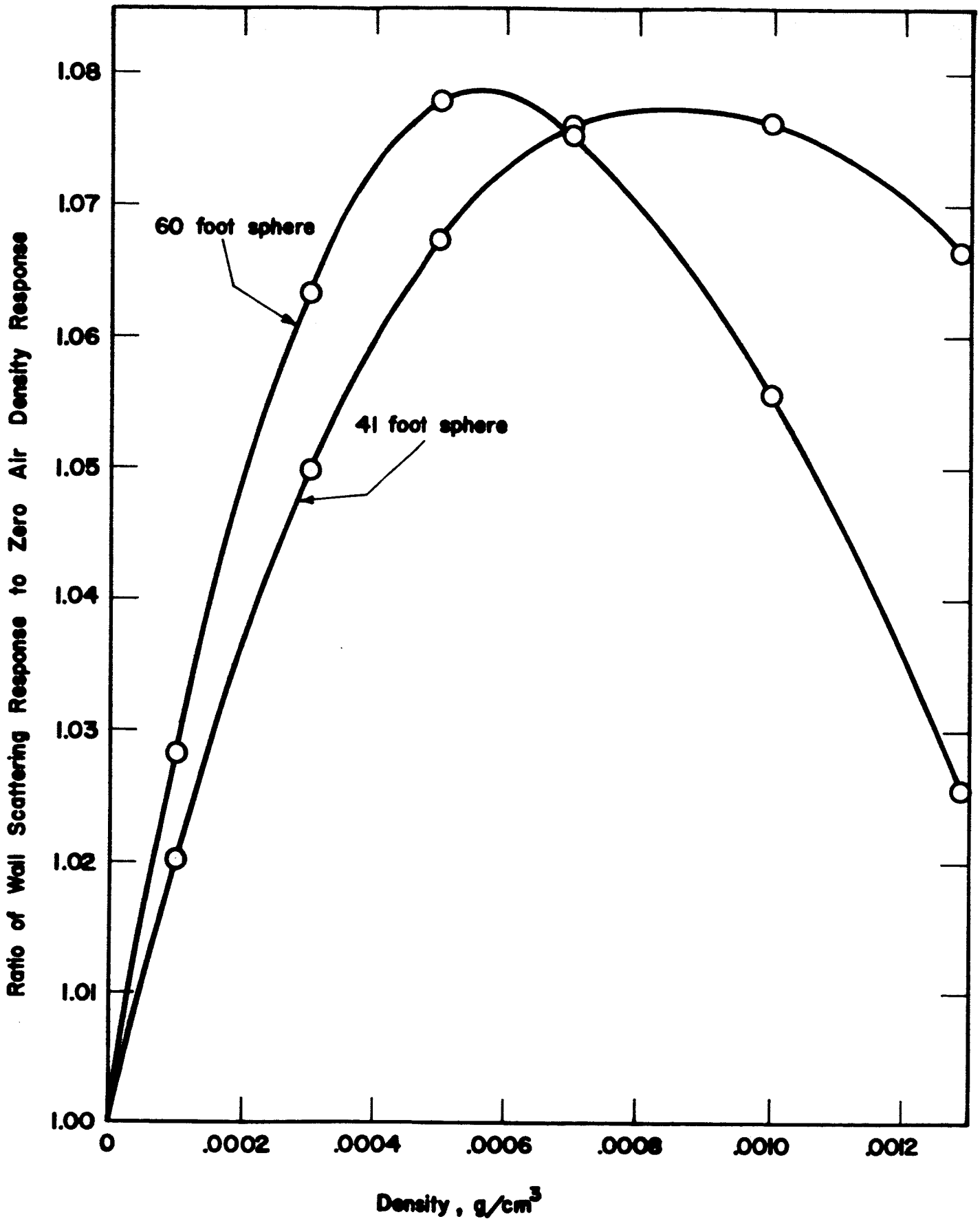

Fig. 7. Predicted gauge responses to wall scattering at various air densities in steel spheres of 60 and 41 foot diameters

Table 1

Dimensions of Prototype Rocket-Mounted Gauge

Item*	Dimension
a_1	.0915
a_2	1.45 cm
d_1	5.08 cm (2.00 in.)
d_i	10.16 cm (4.00 in.)
d	42.23 cm
ϕ_{min}	.785 radians
ϕ_{max}	1.92 radians
t_w	.5588 cm
r_{max}	1000 cm
K	1.01×10^{-33} cm^2 $electron^a$ $atom^{1-a}$ Mev^{-b}
a	5.0
b	3.5

*Refer to Fig. 1 and Sec. 4.1 for a description of these items.

Table 2

Predicted Gauge Response to Atmospheric Density*

Relative Gauge Response	Atmospheric Density (g/cm^3)	Ratio of Response to Density
4.3862	.00300	1462.1
1.9006	.00129	1473.3
1.4753	.00100	1475.3
1.1813	.00080	1476.6
Average		1471.8
Fractional Standard Deviation from Average		±.0045

*The results given here were obtained with the basic model described in Sec. 4.1 with the parameters given in Table 1. In addition the gamma-ray energy of the source was taken as 0.134 Mev, the atmospheric composition was that of air at sea level, and the detector efficiency was the total efficiency as given in Fig. 6. These results are therefore indicative of the prototype gauges with a ^{144}Ce - ^{144}Pr source.

Table 3

Compositions of Earth and Mars Atmospheres

Component	*Mars Atmosphere Mass Fractions	Earth Atmosphere Mass Fractions
CO_2	.700	.001
N_2	.000	.755
A	.300	.013
O_2	.000	.231

*NASA Model IV[4].

Table 4

Effect of Atmospheric Composition on Predicted Gauge Response at Various Gamma-Ray Energies*

Gamma-Ray Energy (Mev)	Relative Gauge Response to Mars Atmosphere	Relative Gauge Response to Earth Atmosphere	Ratio of Mars to Earth Responses
.020	2.36	7.80	.303
.030	6.50	10.00	.650
.050	8.75	9.89	.885
.080	8.33	8.77	.950
.134	6.94	7.18	.967
.300	4.54	4.68	.970
.694	2.64	2.72	.971
2.180	1.122	1.15	.971

*The results given here were obtained with the basic model described in Sec. 4.1 with the parameters given in Table 1. In addition the compositions of the Mars and Earth atmospheres were taken as those given in Table 3 and the detector efficiency was taken as the total efficiency given in Fig. 6.

Table 5

Response Moments of Gauge About the Source as a Function of Source Energy*

Source Energy (Mev)	Lateral Moment, $\bar{x}$[a] (cm)	Vertical Moment, $\bar{y}$[b] (cm)
2.180	24.0	90.5
.694	24.9	98.0
.300	25.5	101.5
.134	25.8	105.5
.080	26.2	110.2
.050	25.9	109.5
.030	24.2	105.6
.020	19.0	94.9

[a]The x distance is measured from the source along the major axis of the rocket in the direction of the detector. Refer to Fig. 1 for a schematic drawing of the rocket and gamma-ray gauge.

[b]The y distance is measured from the source along a line perpendicular to the major axis of the rocket. Refer to Fig. 1 for a schematic drawing of the rocket and gamma-ray gauge.

*The results given here were obtained with the basic model described in Sec. 4.1 with the parameters given in Table 1. In addition the composition and density of the atmosphere was taken as that for air at sea level and the detector efficiency was taken as the total efficiency as given in Fig. 6.

Table 6

Gauge Response as a Function
of Source-to-Detector Distance*

Source Energy (Mev)	Source-to-Detector Distance (cm)	Predicted Relative Gauge Response
0.134	30.48	.117
0.134	42.23	.082
0.134	50.80	.067
0.134	60.96	.055
0.694	30.48	.118
0.694	42.23	.084
0.694	50.80	.068
0.694	60.96	.056
2.180	30.48	.118
2.180	42.23	.084
2.180	50.80	.068
2.180	60.96	.056

*The results given here were obtained with the basic model described in Sec. 4.1 with the parameters given in Table 1. In addition the composition of the atmosphere was taken as that of air at sea level and the detector efficiency was taken as the total efficiency given in Fig. 6.

Table 7

Predicted Effect of Shock Wave
Density Perturbations on Gauge Response*

Mach No.	Half Angle of Shock Wave (degrees)	Average** Density Ratio	Relative Predicted Gauge Response	Error (%)
1.0	90.0	1.000	.19289	0
1.1	62.5	1.033	.19501	1.10
1.2	55.0	1.034	.19626	1.75
1.3	49.2	1.035	.19659	1.92
1.4	44.7	1.036	.19649	1.87
1.5	41.0	1.038	.19602	1.62
2.2	27.0	1.058	.19434	.75
2.6	22.7	1.078	.19362	.38
3.0	19.7	1.103	.19321	.17
4.6	13.2	1.237	.19297	.09

*The results given here were obtained with the basic model described in Sec. 4.1 and the parameters given in Table 1. In addition the gamma-ray energy of the source was taken as 0.134 Mev, the detector efficiency was taken as the total efficiency as given in Fig. 6, and the atmospheric density and composition was taken as that of air at sea level.

**This value is the ratio of the arithmetic average density in the shock wave to the density outside the shock wave assuming that the density inside the shock wave varies linearly with the distance from the rocket surface to the shock wave interface.

Table 8

Response to Gamma-Ray Wall
Streaming as a Function of Source-to-Detector Distance*

Source Energy (Mev)	Source-to-Detector Distance (cm)	Predicted Response per Unit Gamma Ray
0.134	30.48	$.1897 \times 10^{-7}$
0.134	42.23	$.1897 \times 10^{-8}$
0.134	50.80	$.3904 \times 10^{-9}$
0.134	60.96	$.6466 \times 10^{-10}$
0.694	30.48	$.2098 \times 10^{-8}$
0.694	42.23	$.3725 \times 10^{-9}$
0.694	50.80	$.1147 \times 10^{-9}$
0.694	60.96	$.3045 \times 10^{-10}$
2.180	30.48	$.1220 \times 10^{-8}$
2.180	42.23	$.2694 \times 10^{-9}$
2.180	50.80	$.9895 \times 10^{-10}$
2.180	60.96	$.3259 \times 10^{-10}$

*The results given here were obtained with the model described in Sec. 4.3 with the parameters given in Table 1. In addition the detector efficiency was taken as that for discriminator settings of 90 and 155 Kev and a standard deviation of the detector pulse height of 4.24%. This efficiency is quite similar to that for discriminator settings of 80 and 150 Kev as given in Fig. 6.

Table 9

Predicted Prototype Gauge Response to Gamma Rays of ^{144}Ce - ^{144}Pr*

Gamma-Ray Energy (Mev)	Relative Response per Unit Gamma Ray	Gamma-Ray Abundance	Relative Response per Unit Disintegration
0.134	$.5164 \times 10^{-5}$	.300	$.1549 \times 10^{-5}$
0.694	$.5755 \times 10^{-7}$	.020	$.1151 \times 10^{-8}$
2.180	$.6955 \times 10^{-7}$	.030	$.2087 \times 10^{-8}$

*The results given here were obtained with the model described in Sec. 4.1 with the parameters given in Table 1. In addition the composition and density of the atmosphere was taken as that of air at sea level and the detector efficiency was taken as that for discriminator settings of 90 and 155 Kev and a standard deviation of the detector pulse height of 4.24%. This efficiency is quite similar to that for discriminator settings of 80 and 150 Kev as given in Fig. 6.

Table 10

Predicted Prototype Gauge Response to
Wall Scattering in Steel Spheres with Diameters of 60 and 41 Feet*

Sphere Diameter (feet)	Air Density (g/cm^3)	Predicted Gauge Response per Unit Disintegration of ^{144}Ce - ^{144}Pr
41	.0100	$.23313 \times 10^{-6}$
41	.00129	$.54305 \times 10^{-6}$
41	.00100	$.54811 \times 10^{-6}$
41	.000700	$.54805 \times 10^{-6}$
41	.000500	$.54367 \times 10^{-6}$
41	.000300	$.53466 \times 10^{-6}$
41	.000100	$.51958 \times 10^{-6}$
41	.0000100	$.51039 \times 10^{-6}$
41	.00000100	$.50937 \times 10^{-6}$
60	.0100	$.064881 \times 10^{-6}$
60	.00129	$.23800 \times 10^{-6}$
60	.00100	$.24503 \times 10^{-6}$
60	.000700	$.24957 \times 10^{-6}$
60	.000500	$.24990 \times 10^{-6}$
60	.000300	$.24680 \times 10^{-6}$
60	.000100	$.23868 \times 10^{-6}$
60	.0000100	$.23280 \times 10^{-6}$
60	.00000100	$.23211 \times 10^{-6}$

*The results given here were obtained with the model described in Sec. 4.2 for the parameters given in Table 1. In addition the gamma-ray energies and abundances used were those for ^{144}Ce - ^{144}Pr as given in Table 9, the composition of the atmosphere was that of air at sea level, and the detector efficiency was taken as that for discriminator settings of 90 and 155 Kev with a standard deviation of the detector pulse height of 4.24%. This efficiency is quite similar to that for discriminator settings of 80 and 150 Kev as given in Fig. 6.